

Linear Parameter Varying Control for the X-53 Active Aeroelastic Wing

Peter Seiler*, Gary J. Balas† and Andrew Packard‡

Fuel efficiency, endurance, and noise requirements are pushing modern aircraft to lighter, more flexible designs. This causes the structural modes to occur at lower frequencies increasing the coupling with the rigid body dynamics. The traditional approach to handle aeroservoelastic interaction is to design gain-scheduled flight control laws based on the rigid body dynamics and then use filters to avoid exciting the structural modes. This decoupled approach may not be possible in future, more flexible aircraft without reducing the flight control law bandwidth. Linear parameter varying (LPV) techniques provide a framework for modeling, analysis, and design of the control laws across the flight envelope. This paper applies LPV techniques for the roll control of NASA Dryden's X-53 Active Aeroelastic Wing testbed. LPV techniques are first used to analyze a gain-scheduled classical controller. Gain scheduling is still the dominant design method in industrial flight control laws and LPV analysis tools can play an important role in certifying the performance of these systems. Next, an LPV controller is designed and its performance is compared against the gain-scheduled classical controller.

I. Introduction

Increased fuel efficiency and operational range are significant design drivers for modern commercial aircraft, e.g. the Boeing 787. Similar design objectives are also critical for future military aircraft, e.g. the SensorCraft concept aircraft.¹⁻³ In both cases, lighter aircraft are required to meet these objectives. The reduction in weight is typically achieved by reducing the structure in the wings and fuselage of the aircraft. This makes the aircraft more flexible and causes the structural modes to occur at lower frequencies. The main consequence is that lighter, more flexible aircraft have tight coupling between the rigid body and elastic structural modes. This increases the likelihood of adverse aeroservoelastic phenomena including flutter and control surface reversal.

The traditional approach to handle aeroservoelastic interaction is to design the flight control laws based on the rigid body dynamics and then use filters to avoid exciting the structural modes. The control laws are typically designed at various points in the flight envelope and then gain-scheduled by interpolating these point designs. This gain-scheduled approach may not be possible on future, more flexible aircraft for which the structural modes to occur at lower frequencies. The design will need to consider coupling between the rigid body dynamics, structural modes, and the time-varying gain-scheduled controller. Flexible aircraft would significantly benefit from an integrated aeroservoelastic and rigid body control system.

Several issues must be addressed to enable integrated active control to become a reality. First, the aeroelastic effects involve unsteady flows.⁴⁻⁶ In addition, there can be nonlinear effects, e.g. nonlinear coupling between the structural modes and the aerodynamics.^{5,7} Advanced tools are needed to model these effects across the entire flight envelope. A second issue is that an integrated control design must account for the tight coupling between the rigid body and structural modes. This will likely require novel sensors that can measure, in real-time, the aerodynamic flow around the aircraft structures. Such sensors are currently being developed⁴⁻⁶ and new control architectures may be required to take advantage of these novel measurements. A third issue is that analysis tools are required to certify that the designed feedback system meets structural load requirements and is free from aeroservoelastic instabilities. Existing approaches based on robust flutter margins⁸⁻¹⁰ form a starting point but may need to be extended to handle the complexities introduced by the integrated design approach. To summarize, advanced tools are required for modeling, integrated controller synthesis, and analysis of flexible aircraft.

*MUSYN, Inc., peter.j.seiler@gmail.com

†MUSYN, Inc., balas@musyn.com

‡MUSYN, Inc., andrew.packard60@gmail.com

This paper investigates the use of linear parameter varying (LPV) analysis and control techniques for flexible aircraft control. NASA Dryden’s X-53 Active Aeroelastic Wing (AAW) testbed^{22–24} is used to demonstrate the applicability of LPV techniques. The AAW is an experimental flight test capability for aeroservoelastic control research. This paper will focus on roll rate control of the AAW in the supersonic regime.

The remainder of the paper has the following outline. First, a brief review of the AAW program is given in Section II. Next, the AAW rigid body and aeroelastic dynamics are described in Section III. A gain-scheduled classical control law is designed and analyzed in Section IV. Gain-scheduled classical control is the standard in industry for flight control design. LPV analysis tools can play an important role in certifying the performance of these systems and identifying potential issues due to fast variations in the gain scheduling parameters. The LPV analysis tools provide a useful complement to existing approaches, e.g. margin requirements at each flight condition or robust flutter margins.^{8–10} Section V describes an LPV controller for the AAW and compares this design against the gain-scheduled classical design. Finally, conclusions are given in Section VI.

II. Active Aeroelastic Wing

NASA Dryden’s X-53 Active Aeroelastic Wing (AAW)^{22–24} is an experimental flight test capability for aeroservoelastic control research. NASA and the USAF developed this test bed to investigate the use of aeroelastic flexibility for improved performance of high aspect ratio wings. The effectiveness of the conventional aircraft surfaces, e.g. ailerons and trailing edge flaps, is reduced at higher dynamic pressures due to the flexibility of the wing. This can lead to control reversal at sufficiently high dynamic pressures. The standard solution is to reduce wing flexibility by adding structure, and hence additional weight, to the wings.

The main objective of the AAW Flight Research program was to test an alternative concept that uses wing flexibility to improve control effectiveness. The AAW has inner and outer flaps on the leading edge of the wings. Small movements of these surfaces cause the wing to twist in the direction that increases the local angle of attack and induces a rolling moment on the aircraft. These flaps do not undergo a control reversal and, in fact, their effectiveness increases at higher dynamic pressures. Thus the wing flexibility and twist act in a direction beneficial for control.

To test this concept, the AAW wings were modified from the standard F/A-18 wings to reduce the torsional stiffness.²⁴ This increases the wing flexibility and reduces the frequency of the flexible modes. Advanced tools are required to model the aeroelastic effects because they involve unsteady flows^{4–6} and there can be nonlinearities.^{5,7} For control design, linear models of the rigid body and aeroelastic dynamics are obtained at each flight condition via linearization. This naturally falls within the class of linear parameter varying (LPV) models that are scheduled as a function of the flight condition.

The flight-tested AAW control architecture is a modified version of the production F/A-18 control laws.²⁵ The basic architecture uses roll rate feedback to track roll rate commands from the pilot lateral stick inputs. The lateral controller commands the aileron, trailing edge flaps, inner leading edge flaps and outer leading edge flaps. Each surface command is the sum of a proportional roll rate feedback term and a proportional roll rate tracking error term. The control gains were tuned to maximize roll rate performance while satisfying structural load and handling quality requirements.²⁵ The gains were tuned using the multi-objective optimization tool CONDUIT.²⁶ This tool performs nonlinear optimization incorporating results from a high fidelity simulation model.

The AAW control laws were designed and flight tested at separate design points in the flight envelope.²⁷ These control laws were tested during 34 Phase II test flights conducted from December 2004 through March 2005.²⁴ The tests spanned the transonic and supersonic flight conditions and included 360° rolling maneuvers, 5g wind up turns, and 4g rolling pullouts. The flight test program validated the Active Aeroelastic Wing concept and was deemed a success. Additional details on the existing AAW flight control laws and flight tests can be found in.^{24,25,27}

III. AAW Roll Rate Model

The AAW rigid body roll rate dynamics are given by:

$$\dot{p} = L_p(h, M)p + L_\delta(h, M)\delta \quad (1)$$

where p is roll rate (deg/sec) and δ is the outer leading edge flap position (deg). The outer leading edge flap (OLEF) is effective across the supersonic flight envelope of interest. Thus only this surface is used for roll rate control design in this paper. The rigid body LPV model from outer leading edge flap to roll rate (Equation 1) is denoted G_{rig} .

L_p and L_δ are defined on a grid of altitude h (ft) and Mach M (unitless) with values provided in Tables 1 and

2. This data was constructed from non-dimensional aerodynamic coefficients obtained from NASA Dryden.³² The non-dimensional L_δ data was re-scaled to obtain a mean gain of 2 over the flight envelope. Hence the variations of the L_δ data in Table 2 across the flight envelope accurately represent the AAW OLEF gain but the absolute magnitude contains a scaling factor. This scaling will be discussed in the following paragraphs.

	M=1.1	M=1.2	M=1.3
h=10k	-0.5652	-0.4614	-0.4009
h=15k	-0.5415	-0.4363	-0.3737
h=20k	-0.5165	-0.4128	-0.3606
h=25k	-0.5034	-0.3982	-0.3531

Table 1: AAW Rigid Body Data, L_p

	M=1.1	M=1.2	M=1.3
h=10k	1.2916	1.3756	1.2425
h=15k	0.9305	1.0524	1.1958
h=20k	0.6032	0.7009	0.8326
h=25k	0.3056	0.4110	0.5258

Table 2: AAW Rigid Body Data, L_δ

The AAW wings were modified for increased flexibility leading to flexible modes occurring at lower frequencies. Models of the AAW aeroelastic dynamics were obtained from NASA Dryden³² on a grid of altitude, Mach, and remaining fuel. The dependence on remaining fuel is neglected and the models at 60% fuel are used for the design and analysis. The aeroelastic dynamics are defined on the same (h, M) grid used to define the rigid body dynamics, i.e. the aeroelastic dynamics are defined on the grid $h = \{10000, 15000, 20000, 25000\}$ ft and $M = \{1.1, 1.2, 1.3\}$. At each flight condition the aeroelastic dynamics are modeled as a state-space system with 164 states. This model includes 64 states for the first 32 flexible modes and another 100 states for aerodynamic lags. The aerodynamic lag states can be truncated at each point in flight envelope with minimal impact on the OLEF to roll rate dynamics. The resulting aeroelastic model, denoted G_{flex} , has 64 states at each (h, M) flight condition.

The aeroelastic dynamics are added in parallel to the rigid body dynamics to obtain the full 65 state model, $G_{full} = G_{rig} + G_{flex}$. Figure 1 shows the open-loop Bode plots of G_{full} from OLEF to roll rate at each point in the (h, M) domain. As noted above, the L_δ data was rescaled to give a mean gain of 2 across the flight envelope. This effectively increases the significance of the flexible modes relative to the rigid body dynamics. In particular, several of the flexible modes have magnitude exceeding 15dB at points in the flight envelope. The first cluster of flexible modes occur around 55-65 rad/sec. The OLEF actuator has a bandwidth of 75 rad/sec. This bandwidth is not fast enough to actively suppress these flexible modes. The original intent was to use LPV techniques to actively control the AAW flexible modes. The AAW aircraft does not require active attenuation of the flexible modes nor is the OLEF actuator sufficiently fast to suppress these modes. Thus any control law must roll-off to avoid exciting these modes. Since the OLEF actuator dynamics are substantially faster than the AAW roll subsidence mode (L_p) these dynamics will be neglected in most of the design and analysis in the subsequent sections.

IV. Gain Scheduled Classical Control

Gain scheduling via interpolation of point designs is still the predominant method used in industry to develop a full-envelope flight control law. LPV analysis can play an important role in certifying the performance of these control laws. Moreover, LPV analysis tools can uncover potential stability and performance degradations caused by rapid variations in the operating condition. This is especially important for systems with significant aeroelastic effects because flexible modes may be excited during aircraft maneuvers. This section analyzes the performance of a gain scheduled classical roll rate control design using LPV techniques.

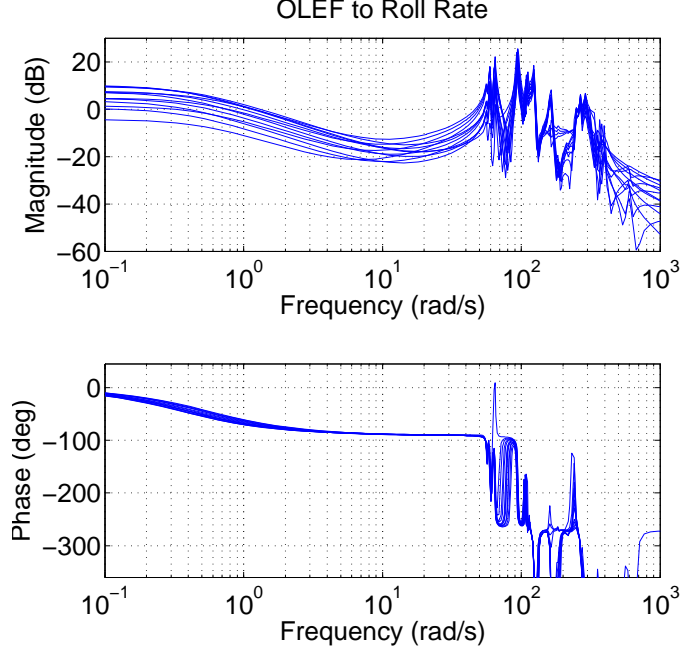


Figure 1: Open loop Bode plots from OLEF to roll rate

A. Control Design

The primary flight control objective is to design a feedback law to track roll rate commands. The variation in the speed of response and gain of the AAW rigid body dynamics across the (h, M) flight envelope (Tables 1 and 2) poses one issue for the control design. The roll subsidence mode varies from -0.56 rad/sec to -0.35 rad/sec and the input gain varies from 0.31 to 1.29. A gain scheduled controller is designed to achieve a consistent bandwidth of 1.25 rad/sec and zero steady state error due to step roll rate commands across the envelope. Another design issue is that the controller must be robust to the flexible modes. The gain scheduled controller is designed so that, in closed-loop, the flexible modes have magnitude less than -20 dB at each point in the flight envelope. This is to ensure the flexible wing modes are not excited by the flight control system. In addition the gain scheduled controller should achieve 6dB of gain margin and 45deg of phase margin at each point in the envelope. These are standard margin requirements for military aircraft. The margin specifications at each point in the envelope essentially assume a quasi-steady approximation for (h, M) . LPV analysis tools will be used to determine the impact of variations in (h, M) on the closed-loop performance.

A classical gain-scheduled controller is designed to achieve these objectives. The basic idea is to invert the rigid body dynamics and replace them with a desired loop shape. In other words, the controller is given by $K_{cl} = G_{inv}G_{ls}$ where G_{inv} inverts the plant dynamics and G_{ls} is the desired loop shape. At each flight condition the AAW rigid body roll-rate dynamics are given by $\frac{L_{\delta}}{s+L_p}$. The rigid body-dynamics are, in general, time-varying due to the dependence on (h, M) and hence the transfer function representation is not correct. However, this representation will be used to provide the basic insight into the control design. The controller inverts the rigid body dynamics up to a bandwidth ω_{ro} to prevent exciting the flexible modes, $G_{inv} = \frac{s+L_p}{L_{\delta}} \frac{\omega_{ro}}{s+\omega_{ro}}$. The roll-off is chosen to be $\omega_{ro} = 12.5$ rad/sec. This is fast enough to have minimal impact on the roll-rate response but slow enough to avoid excessive excitation of the flex modes at 55-65 rad/sec. The desired loop shape is $G_{ls} = \frac{\omega_d^2}{s^2+2\zeta\omega_d}$. The values used in the control design are $\zeta = 0.8$ and $\omega_d = 1.25$ rad/sec. This desired loop shape provides a second order step response with small overshoot, zero steady state error, and a rise time of approximately 2.2 seconds.

As noted above, the plant and controller are both, in general, time-varying systems and transfer function representations are not meaningful. State-space representations should be used instead. The gain scheduled classical

controller $K_{cl} = G_{inv}G_{ls}$ is given by the state-space representations:

$$\left[\begin{array}{c|c} A_{ls} & B_{ls} \\ \hline C_{ls} & D_{ls} \end{array} \right] := \left[\begin{array}{c|c|c} -2\zeta\omega_d & 1 & 0 \\ \hline 0 & 0 & \omega_d \\ \hline \omega_d & 0 & 0 \end{array} \right] \quad (2)$$

$$\left[\begin{array}{c|c} A_{inv} & B_{inv} \\ \hline C_{inv} & D_{inv} \end{array} \right] := \left[\begin{array}{c|c} -\omega_{ro} & \omega_{ro} \\ \hline -\frac{L_p(h,M)+\omega_{ro}}{L_\delta(h,M)} & \frac{\omega_{ro}}{L_\delta(h,M)} \end{array} \right] \quad (3)$$

The dependence on (h, M) has been made explicit for clarity. The controller state matrices are defined on the 4×3 (h, M) grid for which plant data is available (see Tables 1 and 2). The classical controller is gain-scheduled by linearly interpolating the state matrices for G_{ls} and G_{inv} . The realization of G_{inv} in Equation 3 isolates all time-variations in the output and feedthrough matrices. This realization enables to the controller to instantly cancel variations in the plant dynamics. A drawback is that this realization of the controller will be sensitive to errors in the AAW gain-scheduled model.

B. LTI Point Analysis

Insight into the control design and feedback system can be obtained by studying the LTI performance at each point in the flight envelope. Figure 2 shows the Bode plots for the classical controller K_{cl} at each point in the flight envelope. The controller has proportional-integral action at low frequencies with a second order roll-off beyond ω_{ro} to avoid exciting the flexible modes. These Bode plots show an intuitive classical design at each point in the flight domain. In addition, the loop function $G_{full}K_{cl}$ has significant attenuation of the flexible modes in comparison with the open loop Bode G_{full} . The loop $G_{full}K_{cl}$ has all modes below -19dB at all points in the flight envelope. In closed loop the flexible modes are still well attenuated. The closed-loop response from roll rate command to roll rate has the flexible modes below -18.5dB at all points in the domain. The loop function $G_{full}K_{cl}$ has gain and phase margins exceeding 21.3dB and 65.9 degs at each point in the flight domain. Thus the classical controller has good gain and phase margins at each point in the flight envelope.

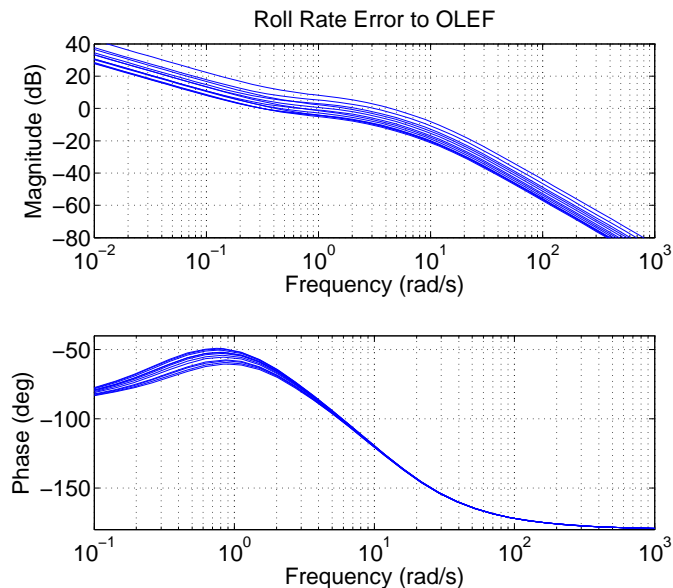


Figure 2: Bode plots of classical controller

Figure 3 shows the closed-loop unit step responses to a 1 deg roll rate command at all points in the flight envelope. The full model with flexible modes G_{full} and gain-scheduled classical controller K_{cl} are used to generate these closed-loop responses. The left plot shows the roll rate response and the right plot shows the OLEF position. The blue solid curve in the left plot shows the ideal closed-loop response given by the open loop specification G_{ls} . The red dashed curves in both plots show the closed loop responses at each point in the (h, M) domain. The classical controller

achieves consistent dynamic performance across the flight envelope with zero steady state error (left plot). The right plot shows the variation in the control actuation required to achieve this uniform tracking performance. In addition, the closed loop step responses (left plot of Figure 3) indicate only small oscillations in the initial transient due to the flexible modes. This is due to the high frequency roll-off of K_{cl} which attenuates the flexible modes. Finally, the closed-loop responses (left plot) have a small deviation from the ideal response. This is due to the high-frequency roll-off in G_{inv} to avoid exciting the flexible modes.

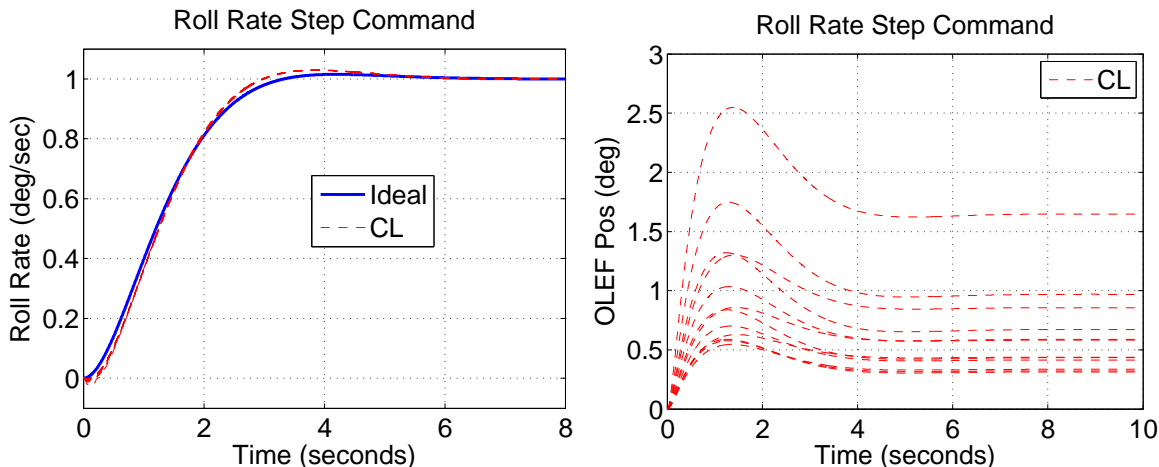


Figure 3: Closed-loop responses to step roll rate command with K_{cl}

The closed-loop performance can be evaluated using the induced L_2 norm of various closed-loop sensitivity functions in the feedback loop. Table 3a shows results computed for the feedback system consisting of the rigid body dynamics G_{rig} and the gain-scheduled classical controller K_{cl} . The rows labeled S_i , T_i , S_o , and T_o provide induced L_2 norm bounds for the input sensitivity, input complementary sensitivity, output sensitivity, and output complementary sensitivity. The second column, labeled Point H_∞ , is the maximum H_∞ norm over all points in the flight envelope. For the row labeled S_i , this result was obtained by computing the H_∞ norm of the input sensitivity function at each point in the flight envelope and then maximizing over the flight envelope. The results in the other rows were obtained similarly. Each data point in this column took, on average, 0.21 seconds to compute on a laptop with a dual-core 2.16GHz Intel processor. At a fixed point in the flight envelope, the H_∞ norm for each sensitivity function is equal to its induced L_2 norm. This is a lower bound on the actual induced L_2 norm for the gain-scheduled system since it does not account for parameter variations. The results for the input and output functions are equal because the feedback loop is SISO and the point-wise H_∞ norm assumes time-invariant dynamics at each point in the domain. The remaining columns in Table 3a are discussed in the following subsection.

The pointwise H_∞ analysis can also be used to investigate the impact of the flexible modes at each point in the domain. The full model G_{full} with rigid body and aeroelastic dynamics has 65 states. For this analysis a reduced order model, G_{red} , that captures the first three flexible modes was constructed by residualizing the higher frequency flexible modes at all points in the flight envelope. G_{red} has a total of seven states: one state for the rigid body dynamics and six states for the first three flexible modes. The closed loop sensitivity functions are then formed with G_{red} and K_{cl} . Table 3b shows the various norms computed for the closed loop sensitivity functions with G_{red} and K_{cl} . The rows and columns of this table can be compared with the previous analysis for the closed loop with the rigid body dynamics (Table 3a). The maximum H_∞ norm over the flight envelope (column: Point H_∞) shows only minor differences with the results for the rigid body dynamics. Thus the H_∞ norms computed at each point in the flight domain indicate that the aeroelastic dynamics will have minimal impact on the gain scheduled performance.

C. LPV Analysis

The analysis of the gain-scheduled classical controller has, up to this point, focused on the performance at each point in the (h, M) flight envelope. This analysis neglects the impact of time variations in altitude and Mach. The induced L_2 norm for an LPV system is the maximum input/output gain over all inputs and a class of allowable parameter trajectories. A generalization of the Bounded Real condition leads to linear matrix inequality (LMI) conditions for computing bounds on the induced L_2 norm. These parameterized LMI conditions are based on results in.¹⁴

Closed-loop with (G_{rig}, K_{cl})					Closed-loop with (G_{red}, K_{cl})				
	Point H_∞	LPV1	LPV2	LPV3		Point H_∞	LPV1	LPV2	LPV3
S_i	1.292	3.786	2.222	1.590	S_i	1.314	Inf	2.202	1.548
T_i	1.000	3.685	2.116	1.431	T_i	1.000	Inf	2.143	1.418
S_o	1.292	1.295	1.296	1.298	S_o	1.314	Inf	2.406	1.347
T_o	1.000	1.000	1.000	1.001	T_o	1.000	Inf	2.096	1.009

(a)

(b)

Table 3: L_2 induced norms for closed-loop sensitivity functions with gain-scheduled classical controller

Upper bounds on the induced L_2 norm of the various closed-loop sensitivity functions were computed to gain insight into the effect of variations in (h, M) . The results for the closed loop with G_{rig} and K_{cl} are given in the columns LPV1, LPV2, and LPV3 of Table 3a. The results in these columns involve LPV induced L_2 norm upper bounds of various complexity. The column labeled LPV1 used constant Lyapunov matrices in the induced L_2 norm LMI conditions. This is equivalent to an analysis that assumes no knowledge of the parameter rates. The results in columns LPV2 and LPV3 both assume the rate bounds $|\dot{M}| \leq 0.02$ 1/sec and $|\dot{h}| \leq 1000$ ft/sec. LPV2 uses a parameter dependent Lyapunov function of the form $X(\rho) = X_0 + MX_1 + hX_2$ while LPV3 also includes quadratic bases functions, $X(\rho) = X_0 + MX_1 + hX_2 + M^2X_3 + MhX_4 + h^2X_5$. In theory the upper bounds on the induced L_2 norm should progressively decrease from analysis LPV1 to LPV2 to LPV3. The results for S_o and T_o in Table 3a do not demonstrate this theoretical trend but the results are within the stopping tolerances of the optimization solver.

There are several interesting aspects to the LPV analysis results in Table 3a. First, the output sensitivity functions, S_o and T_o , have an induced norm almost exactly equal to the pointwise H_∞ lower bound. This is because the classical controller perfectly cancels the rigid body dynamics for reference commands that enter at the plant output. However, the cancellation is not perfect for disturbances that enter at the plant input. Thus there is a gap between the upper bounds for S_i and T_i and the pointwise H_∞ lower bounds. The gap is reduced by including additional bases functions in the LPV analysis. The price paid for this improved upper bound is an increased computational complexity. Each LPV1, LPV2, and LPV3 analysis took 0.75, 10.1, and 37.6 seconds, on average. These results indicate that the variations in (h, M) are unlikely to affect the reference tracking but it may have some effect on disturbance rejection at the plant input.

The LPV analysis can also be used to investigate the impact of the flexible modes. As described in the previous subsection, a reduced order, 7-state aeroelastic model was obtained by retaining the first three flexible modes in the full model. This model reduction was mainly motivated by the computational complexity of the LPV analysis condition with respect to the plant state dimension. The 65-state model G_{full} is too large to be handled by current optimization solvers but the 7-state reduced order model can be analyzed in a reasonable amount of time. Columns LPV1, LPV2, and LPV3 in Table 3b shows the LPV upper bounds computed for the closed loop sensitivity functions with G_{red} and K_{cl} . The rows and columns of this table can be compared with the previous analysis for the closed loop with the rigid body dynamics (Table 3a). The LPV upper bounds computed with using linear and quadratic basis functions (column LPV3 in Table 3b) are roughly the same as the results obtained with the rigid body dynamics (column LPV3 in Table 3a). This indicates that the aeroelastic dynamics will have minor impact the gain-scheduled closed-loop performance. This agrees with the results obtained using pointwise H_∞ norms. The results labeled Inf in column LPV1 indicate that no provable upper bound on the induced L_2 norm can be obtained using constant, quadratic Lyapunov functions.

The LPV analysis (Tables 3a and 3b) has gaps between the pointwise H_∞ lower bounds and the LPV3 analysis upper bound. The user could continue adding bases functions and see if the LPV3 analysis bound can be reduced. However, there is a computational penalty to be paid for adding bases functions. Each Point H_∞ , LPV1, LPV2, and LPV3 analysis in Table 3b took 0.08, 0.58, 91.6 and 360.6 seconds, on average. An alternative is to compute improved lower bounds via simulation.

V. LPV Control Design

This section describes an LPV control design that provides guaranteed performance with respect to time variations in the (h, M) parameters. The design approach is based on signal-weighted induced L_2 norms. Figure 4 shows the

design interconnection used for the control synthesis. The performance objective is to minimize the induced L_2 norm from the design interconnection inputs to the outputs. The various I/O signals are weighted to obtain the desired trade-offs between reference tracking, disturbance/noise rejection, and actuation usage.

The rigid body AAW dynamic models G_{rig} are used in the design. The design interconnection formulates a model-matching problem. The key performance objective is for the closed-loop response from p_{cmd} to p to match the ideal response given by $G_{ideal} = \frac{\omega_d^2}{s^2 + 2\zeta\omega_d s + \omega_d^2}$. The ideal response natural frequency and damping are given by $\zeta = 0.8$ and $\omega_d = 1.25$ rad/sec. This is the same ideal response given by the loop shape G_{ls} in the gain-scheduled classical design. The actuation and performance penalties are given by $W_a = \frac{100s+25}{s+2500}$ and $W_p = \frac{0.01s+12.5}{s+0.125}$. This emphasizes tracking of the ideal response up to ≈ 11.25 rad/sec and penalizes control usage at higher frequencies. The input disturbance and noise weights are chosen as $W_d = 0.1$ and $W_n = 0.01$. The small values are chosen to emphasize the actuation / performance trade-off. The ideal model and all weights are independent of the flight condition. Thus the performance objective aims to achieve similar performance across the flight envelope.

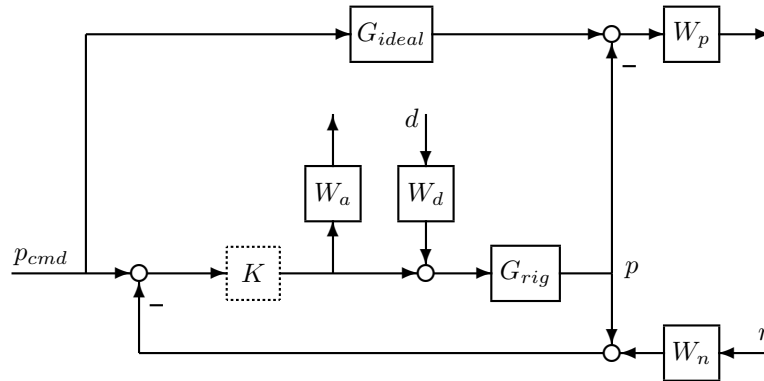


Figure 4: Design interconnection AAW roll rate control

To understand the limits of performance, the H_∞ optimal control problem specified by this design interconnection was solved at each point in the flight envelope. The optimal performance varied from a minimum of $\gamma = 1.008$ at $(h, M) = (25000ft, 1.1)$ to a maximum of $\gamma = 3.726$ at $(h, M) = (15000ft, 1.3)$. The optimal performance of any LPV design must be greater than or equal to the optimal H_∞ performance achieved at any point in the domain. Hence $\gamma = 3.726$ is a lower bound on the achievable performance by the optimal LPV controller. For comparison, the gain-scheduled classical controller, K_{cl} , achieves a minimum gain of $\gamma = 1.000$ at $(h, M) = (25000ft, 1.1)$ and a maximum gain of $\gamma = 3.857$ at $(h, M) = (15000ft, 1.3)$.

Next, an LPV controller was synthesized without using knowledge about the rate variations of altitude and Mach. This control synthesis is performed by solving a set parameterized LMIs using a constant (non-parameter varying) Lyapunov function. The parameterized LMI conditions are based on results in.¹⁴ The non-rate bounded bounded design achieves an optimal gain of $\gamma_{lpv,nr} = 3.844$. This is very close to the performance lower bound computed based on the point-wise H_∞ designs. The design interconnection has a total of five states: one for the rigid body AAW dynamics, two for the ideal response model and one each for the actuation and performance weights. The non-rate bounded controller K_{lpv} has the same number of states as the design interconnection, i.e. K_{lpv} has five states. A rate-bounded LPV controller was also synthesized assuming $|\dot{M}| \leq 0.02$ and $|\dot{h}| \leq 1000$ ft/sec and using basis functions $\{1, M, h\}$. The rate bounded design achieved a gain of $\gamma_{lpv,rb} = 3.797$. This is a small improvement over the non-rate bounded design. Hence the bound on the rate of the parameter variation does not play a significant role in the AAW design. The remainder of the section will focus on the non-rate bounded control design.

Figure 5 shows the Bode plots for the the non-rate bounded LPV controller K_{lpv} at each point in the flight envelope. The controller has proportional-integral action at low frequencies and a second order roll-off beyond ω_{ro} to avoid exciting the flexible modes. Both these characteristics are similar to gain-scheduled classical design shown in Figure 2. One difference is that K_{lpv} has additional phase lead between 1 to 10 rad/sec. In addition, K_{lpv} has the same high frequency gain at all points in the flight envelope while the high frequency gain of the classical design K_{cl} varies with the flight condition. The point-wise Bode plots of K_{lpv} show an intuitive classical design at each point in the flight domain.

The loop $G_{full}K_{nr}$ attenuates all modes below -12.0dB at all points in the flight envelope. In closed-loop, the response from roll rate command to roll rate has the flexible modes below -12.4dB at all points in the domain. This

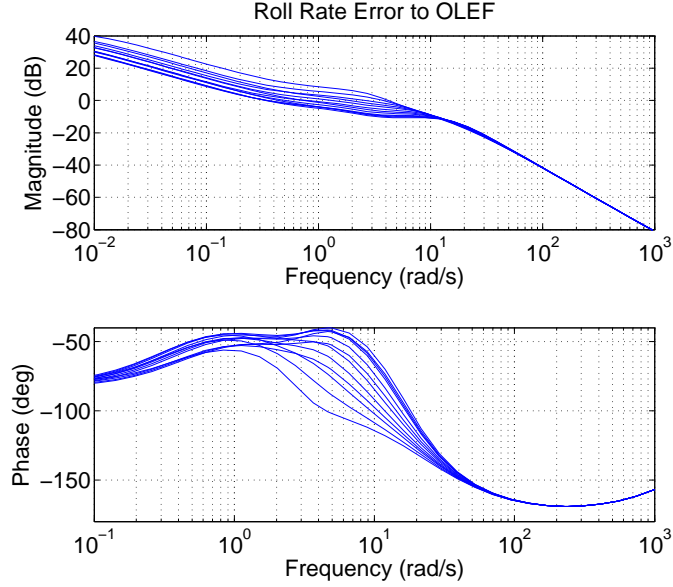


Figure 5: Bode magnitude plots of LPV controller

is slightly less attenuation than achieved by the gain-scheduled classical controller. The additional phase lead in K_{nr} is evident from 1 to 10 rad/sec in the Bode plot of $G_{full}K_{nr}$. The loop function $G_{full}K_{cl}$ has gain and phase margins exceeding 18.8dB and 66.7 degs at each point in the flight domain. This is a slightly smaller gain margin than K_{cl} but the phase margins of K_{cl} and K_{nr} are essentially the same.

Figure 6 shows the closed-loop unit step responses to a 1 deg roll rate command at all points in the flight envelope. The full model with flexible modes G_{full} and LPV controller K_{nr} are used to generate these closed-loop responses. The left plot shows the roll rate response and the right plot shows the OLEF position. The blue solid curve in the left plot shows the ideal closed-loop response specified by the ideal model G_{ideal} . The red dashed curves in both plots show the closed loop responses at each point in the (h, M) domain. The LPV controller achieves consistent dynamic performance across the flight envelope with good attenuation of the flexible modes. The LPV controller provides slightly better tracking of the ideal response when compared to the classical design (Figure 3). Both K_{nr} and K_{cl} have similar actuator usage for the step roll rate command.

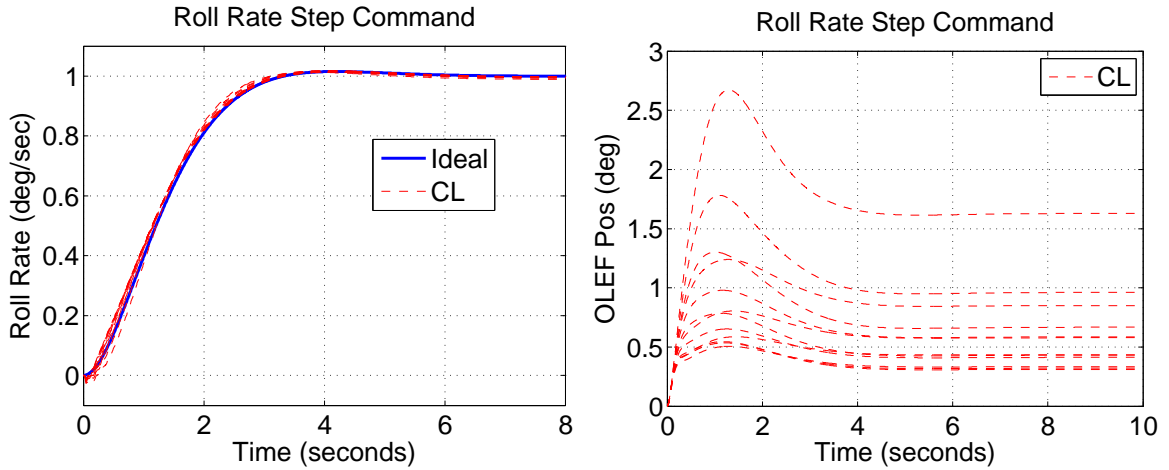


Figure 6: Closed-loop responses to step roll rate command with K_{nr}

Tables 4a and 4b show the bounds on the LPV induced L_2 norms of the various closed-loop sensitivity functions.

Table 4a was computed using G_{rig} and K_{lpv} while the results in Table 4b were computed with the reduced aeroelastic model G_{red} and K_{lpv} . These results can be compared with the gain scheduled classical controller performance K_{cl} in Tables 3a and 3b. The LPV controller has slightly achieves slightly better performance based on the rate-bounded upper bounds computed using the linear and quadratic basis functions (column LPV3).

Closed-loop with (G_{rig}, K_{lpv})					Closed-loop with (G_{red}, K_{lpv})				
	Point H_∞	LPV1	LPV2	LPV3		Point H_∞	LPV1	LPV2	LPV3
S_i	1.302	3.682	2.063	1.434	S_i	1.328	Inf	2.087	1.450
T_i	0.995	3.586	2.004	1.358	T_i	0.995	Inf	2.036	1.360
S_o	1.302	1.315	1.309	1.306	S_o	1.328	Inf	1.356	1.357
T_o	0.995	1.002	0.998	0.998	T_o	0.995	Inf	1.007	0.999

(a)

(b)

Table 4: L_2 induced norms for closed-loop sensitivity functions with LPV controller

VI. Conclusions

This paper investigated the use of LPV techniques for the roll control of NASA Dryden’s X-53 Active Aeroelastic Wing (AAW) testbed. LPV analysis of a gain-scheduled classical controller indicated that variations in scheduling parameter would have minimal impact on reference tracking but may have some impact on disturbance rejection at the plant input. An LPV controller was also synthesized using a model matching design. The LPV controller has an intuitive classical control characteristics and its performance was similar to the gain-scheduled classical design.

VII. Acknowledgments

This research was supported under the NASA Dryden SBIR NNX11CD58P entitled “Adaptive Linear Parameter-Varying Control for Aeroelastic Suppression”. The technical contract monitor is Dr. Martin J. Brenner.

References

- ¹D. Lucia, “The sensorcraft configurations: A non-linear aeroservoelastic challenge for aviation,” in *AIAA/ASME/ASCE/AHS/ASC Structures, Structural Dynamics and Materials Conference and Exhibit*, no. AIAA-2005-1943, 2005.
- ²J. Martinez, P. Flick, J. Perdsock, G. Dale, and M. Davis, “An overview of sensorcraft capabilities and key enabling technologies,” in *AIAA Applied Aerodynamics Conference*, no. AIAA-2008-7185, 2008.
- ³E. Vartio, A. Shimko, C. Tilman, and P. Flick, “Structural mode control and gust alleviation for a sensorcraft concept,” in *AIAA/ASME/ASCE/AHS/ASC Structures, Structural Dynamics and Materials Conference and Exhibit*, no. AIAA-2005-1840, 2005.
- ⁴A. Mangalam and T. Moes, “Real-time unsteady loads measurements using hot-film sensors,” in *AIAA Applied Aerodynamics Conference*, no. AIAA 2004-5371, 2004.
- ⁵S. Mangalam, P. Flick, and M. Brenner, “Higher level aerodynamics input for aeroservoelastic control of flexible aircraft,” in *AIAA Atmospheric Flight Mechanics Conference*, no. AIAA 2007-6380, 2007.
- ⁶A. Mangalam, S. Mangalam, and P. Flick, “Unsteady aerodynamic observable for gust load alleviation and flutter suppression,” in *AIAA Atmospheric Flight Mechanics Conference*, no. AIAA 2008-7187, 2008.
- ⁷B. Boehm, P. Flick, B. Sanders, C. Pettit, E. Reichenbach, and S. Zillmer, “Static aeroelastic response predictions of the active aeroelastic wing (AAW) flight research vehicle,” in *AIAA/ASME/ASCE/AHS/ASC Structures, Structural Dynamics & Materials Conference*, no. AIAA 2001-1372, 2001.
- ⁸M. Brenner and R. Lind, “Wavelet-processed flight data for robust aeroservoelastic stability margins,” *AIAA Journal of Guidance, Control, and Dynamics*, vol. 21, no. 6, pp. 823–829, 1998.
- ⁹R. Lind and M. Brenner, “Analyzing aeroservoelastic stability margins using the μ method,” in *AIAA Structures, Structural Dynamics, and Materials Conference*, no. AIAA 98-1895, 1998, pp. 1672–1681.
- ¹⁰M. Brenner, “Aeroservoelastic model uncertainty bound estimation from flight data,” *AIAA Journal of Guidance, Control, and Dynamics*, vol. 25, no. 4, pp. 748–754, 2002.
- ¹¹J. Shamma and M. Athans, “Gain scheduling: potential hazards and possible remedies,” in *American Control Conference*, 1991, pp. 516–521.
- ¹²A. Packard and M. Kantner, “Gain scheduling the LPV way,” in *IEEE Conference on Decision and Control*, 1996, pp. 3938–3941.
- ¹³S. Sharuz and S. Behtash, “Design of controllers for linear parameter-varying systems by the gain-scheduling technique,” in *IEEE Conference on Decision and Control*, 1990, pp. 2490–2491.

- ¹⁴F. Wu, "Control of linear parameter varying systems," Ph.D. dissertation, University of California, Berkeley, 1993.
- ¹⁵G. Becker, "Quadratic stability and performance of linear parameter dependent systems," Ph.D. dissertation, University of California, Berkeley, 1993.
- ¹⁶P. Apkarian and P. Gahinet, "A convex characterization of gain-scheduled H_∞ controllers," *IEEE Transactions on Automatic Control*, vol. 40, no. 5, pp. 853–864, 1995.
- ¹⁷F. Wu, X. Yang, A. Packard, and G. Becker, "Induced l_2 norm control for LPV systems with bounded parameter variation rates," *International Journal of Nonlinear and Robust Control*, vol. 6, pp. 983–998, 1996.
- ¹⁸A. Packard, "Gain scheduling via linear fractional transformations," *Systems and Control Letters*, vol. 22, no. 2, pp. 79–92, 1994.
- ¹⁹C. Scherer and S. Weiland, *Linear Matrix Inequalities in Control*. DISC Lecture Notes, 2000.
- ²⁰C. Scherer, "LPV control and full block multipliers," *Automatica*, vol. 37, no. 3, pp. 361–375, 2001.
- ²¹J. Veenman and C. Scherer, "On robust LPV controller synthesis: A dynamic integral quadratic constraint based approach." in *IEEE Conference on Decision and Control*, 2010, pp. 591–596.
- ²²E. Pendleton, K. Griffin, M. Kehoe, and B. Perry, "A flight research program for active aeroelastic wing technology," in *AIAA/ASME/ASCE/AHS/ASC Structures, Structural Dynamics and Materials Conference and Exhibit*, 1996, paper 96-1574-CP.
- ²³E. Pendleton, D. Bessette, P. Field, G. Miller, and K. Griffin, "Active aeroelastic wing flight research program: Technical program and model analytical development," *Journal of Aircraft*, vol. 37, no. 4, pp. 554–561, 2000.
- ²⁴E. Pendleton, P. Flick, D. Voracek, E. Reichenbach, K. Griffin, and D. Paul, "The X-53: A summary of the active aeroelastic wing flight research program," in *AIAA Structures, Structural Dynamics, and Materials Conference*, 2007, paper 2007-1855.
- ²⁵R. Dibley, M. Allen, R. Clarke, J. Gera, and J. Hodgkinson, "Development and testing of control laws for the active aeroelastic wing program," NASA, Tech. Rep. TM-2005-213666, 2005.
- ²⁶M. Tischler, J. Colbourne, M. Morel, D. Biezad, W. Levine, and V. Moldoveanu, "CONDUIT: A new multidisciplinary integration environment for flight control development," in *AIAA Guidance, Navigation, and Control Conference*, no. AIAA-1997-3773, 1997.
- ²⁷R. Clarke, M. Allen, R. Dibley, J. Gera, and J. Hodgkinson, "Flight test of the F/A-18 active aeroelastic wing airplane," NASA, Tech. Rep. TM-2005-213664, 2005.
- ²⁸X. Sun and I. Postlethwaite, "Affine LPV modeling and its use in gain-scheduled helicopter control," in *UKACC International Conference on Control*, 1998, pp. 1504–1509.
- ²⁹G. Balas, J. Bokor, and Z. Szabo, "Invariant subspaces for LPV systems and their applications," *IEEE Transactions on Automatic Control*, vol. 48, no. 11, pp. 2065–2069, 2003.
- ³⁰F. Bruzelius and C. Breitholtz, "Gain scheduling via affine linear parameter-varying systems and h_∞ synthesis," in *IEEE Conference on Decision and Control*, 2001, pp. 713–718.
- ³¹P. Baranyi, Y. Yam, and P. Varlaki, *Tensor Product Model Transformation in Polytopic Model-Based Control*. Taylor & Francis, 2011.
- ³²M. Brenner, 2011, Personal Communication.
- ³³P. Gahinet, A. Nemirovski, A. Laub, and M. Chilali, "LMI control toolbox user's guide," The Mathworks, Tech. Rep., 1995.